12-2015

Control of Cation Ordering in Zinc Tin Nitride and In-Situ Monitoring of Growth

Brian Christopher Durant

CONTROL OF CATION ORDERING IN ZINC TIN NITRIDE AND IN-SITU MONITORING OF GROWTH

by

Brian Christopher Durant

A thesis submitted to the Graduate College
in partial fulfillment of the requirements
for the degree of Master of Science in Engineering
Electrical and Computer Engineering
Western Michigan University
December 2015

Thesis Committee

Steven Durbin, Ph.D., Chair
Ralph Tanner, Ph.D
Muralidhar Ghantasala, Ph.D

CONTROL OF CATION ORDERING IN ZINC TIN NITRIDE AND IN-SITU MONITORING OF GROWTH

Brian Christopher Durant, M.S.E

Western Michigan University, 2015

Semiconducting materials with a band gap around 1.5 eV are very much sought after due to their close match to the solar spectrum. However, some compounds that have shown promise for highly efficient solar cells contain rare, expensive, and sometimes toxic elements, such as indium and gallium. As such, a search for earth abundant materials has become more prominent recently. One such earth abundant semiconducting material that has garnered interest is $ZnSnN_2$. It has been shown through previous studies that there is the possibility of continuously tuning the band gap between 1.0 and 2.0 eV by controlling the ordering of the cation sub lattice. In this work, $ZnSnN_2$ is grown under varying growth conditions in an attempt to obtain a fully ordered cation sub lattice. The lattice structure is monitored in real time through in-situ RHEED measurements. After growth, the RHEED patterns are analyzed to extract structural data.

ACKNOWLEDGEMENTS

I would like to thank my advisor, Dr. Steven M. Durbin. Without his support, I would never have thought to make it as far as I have in the search for knowledge. Education has always been my way of life and it was through Durbin's guidance, patience, and professional friendship that the work you see before you today was accomplished. I also want to thank the thesis committee who took time out to come hear my defense and give me great pointers and constructive criticism on my work. I also thank my committee for supporting me throughout my time as a master's student. A special thanks goes to the research lab crew who taught me everything I know today! I wouldn't have been able to do it without Nathaniel Feldberg, Robert Makin, and Benjamin Keen. I know that teaching me wasn't always the best experience. I would also like to thank the National Science Foundation for their funding and for the opportunity for allowing me to continue research in my field of study. Last, but definitely not least, I would like to thank my parents who have supported me through everything I've done in life and raised me to be the man I am today. Thanks guys!

Brian C. Durant

TABLE OF CONTENTS

LIST OF TABLES

LIST OF FIGURES

1.1 Overview of PN Junction Solar Cells

The most common source of electricity up until recent years has been coal, a source that isn't renewable. In fact, coal is very harmful to the environment, which is a main reason for the emergence of alternate forms of energy such as wind, water and solar energy. Renewable energy has been a hot topic in the scientific community ever since the discovery of the photovoltaic effect by Edmund Becquerel in 1839 [1]. At the age of 19, Edmund Becquerel conducted an experiment in which silver chloride was placed in an acidic solution and illuminated while connected to platinum electrodes [1]. This experiment resulted in the generation of a voltage and a current. This phenomenon which occurred is recorded as the photovoltaic effect: the ability to transform photons, or light energy, into voltage and current. Because of his significant contribution to the field, the photovoltaic effect is also known as the "Becquerel effect." [1] The existence of a method to generate a current from a light source opened up many venues for clean energy– energy that produces heat or electricity from renewable resources while generating little or no pollution or emissions.

In the mid-1930s, Russel Ohl and others started experimenting with the use of crystals as rectifiers for radars and radio usage. In the process of these experiments, on February 23, 1940, as Ohl was testing a small silicon slab, he obtained surprising results. When exposed to light, it was seen that there was a significant current flowing through the silicon slab [2]. It was also noted that different parts of the crystal exhibited different

properties when probed with a so-called “cat’s whisker” probe. Upon further inspection, Ohl and his companions realized that a seam in the slab marked the boundary that separated regions of different impurities. One region was doped with phosphorous impurities and the other side was doped with boron impurities. The phosphorous doped region yielded excess electrons in the material while the boron doped region yielded excess holes in the material. Diffusion between the two layers led to formation of a depletion region and an electric field capable of separating photo-generated electron-hole pairs. After attaching probes to this material and measuring the voltage, Ohl and his companions realized that they were getting as much as half a volt out of the device [2]. This is the first known silicon based PN junction and silicon based photovoltaic effect.

Ever since the discovery of the photovoltaic effect, solar cells have seen major use in just about every path of life, from space exploration to powering up hand held calculators. One would expect solar cells to be used everywhere; a device that can generate electricity from the light of the sun is as clean of a source as one might imagine. However, when discussing the manufacturing of solar cells, there are many other factors that need to be considered outside of its use. How much does it cost to produce these solar cells? How much pollution is being created by the fabrication of one of these cells? Can an expired device be recycled? Are the solar cells themselves efficiently converting energy?

One of the first things to consider in the mass production of a new material is its production cost. In the case of solar cells, one must consider whether or not they are created of earth abundant elements, if their production costs are relatively low, and if their manufacture generates significant pollution. One scientist, Elliot Berman, actively worked to make cheaper solar cells due to an estimation that the cost of power would be roughly

$20 per watt of energy by the year 2000 [3,4]; a price this low would make the renewable energy field very attractive. Berman founded and ran a new corporation, Solar Power Corporation, which was backed by ESSO, the international corporation associated with ExxonMobil. Solar Power Corporation worked to make solar cells cheaper and "more efficient" by simplifying the design of space grade solar cells, basically making them of less quality material. New materials were used to create the PN junctions needed to create solar cells and advanced processing steps such as polishing and antireflective layer application were eliminated. It was through his effort and those of big companies who decided to also join in on the future of renewable energy that the price of solar cells started coming down [4].

Modern solar cells are constructed using n-type and p-type layers of one or more semiconductor materials to construct a p-n junction device (high efficiency designs may "stack" multiple junctions, each tuned to part of the solar spectrum). Due to this, the price of solar cells could be directly related to Moore's law. The law relating the two is called Swanson's law [5], which states that assuming the current trend, solar cell prices will fall for 20% for every doubling of industry capacity.

In order to understand how solar cells work, we need to understand the most fundamental characteristic of a semiconductor – its band gap energy, often referred to simply as band gap, and abbreviated Eg. A band gap is the energy difference between the top of the valence band (the highest energy band filled at 0 K) and the bottom of the conduction band (the next highest band). In an insulator, the band gap is very large, generally above 6 eV, while in semiconductors, the band gap ranges from above 0 eV to approximately 6 eV. Band gaps can be indirect or direct. An indirect band gap is generally

seen as a poor attribute for photovoltaic applications because of the corresponding poor absorption of light. When light energy is introduced to a semiconductor, an electron is kicked out of the valence band and into the conduction band (if the energy provided to the electron is equal to or exceeds that of the band gap of the semiconductor material), leaving a hole in the valence band. Thus, photon absorption can lead to generation of an electron-hole pair. However, if the photon energy is less than the band gap, it cannot promote a valence band electron to the conduction band (although the photon may be absorbed by a conduction band electron). After being promoted to the conduction band, the electron attempts to fall back to its original state in the valence band by releasing the energy it obtained from the photon. If an electron receives excessive energy, it doesn't just jump to the conduction band, it jumps even further and then quickly settles back down to the conduction band by releasing the excess energy through lattice vibrations, generating heat. Essentially all the extra energy that was imparted to the electron therefore is wasted.

Another important issue is the doping of the semiconductor material. A pure, undoped semiconductor sample should have equal numbers of electrons and holes. The most commonly used semiconductor currently is silicon. Silicon is a group 4 element with 14 electrons. Ten of these electrons are bound tightly to the atom itself and as such aren't available for bonding. However, four of these atoms lie on the outer shell of the atom, and as such, are called bonding or covalent electrons. When multiple silicon atoms are put together, they form a silicon crystal where the four covalent electrons bond with four covalent electrons from other silicon atoms forming strong covalent bonds. To introduce an excess of electrons into a semiconductor, impurities with a higher number of covalent electrons must replace some of the pure atoms in a crystal. For example, if a silicon crystal

is being used, some of the silicon atoms must be replaced with an atom from group 5 on the periodic table. Four of the dopant atom electrons participate in bonding, and the fifth is available to be "donated" to the conduction band (it is only weakly bound to the donor impurity atom). In the same fashion as n-type doping, we must replace some of the silicon atoms with group 3 elements ("acceptor atoms") in order to create a surplus of holes. Generally, only one atom per one million pure semiconductor atoms are replaced. If the dopant concentration is excessive, the material is most likely better considered an alloy.

After obtaining an n-type and a p-type semiconductor layer, conjoining the two leads to diffusive flow. The result is the leaving behind of positively charged donor (n-

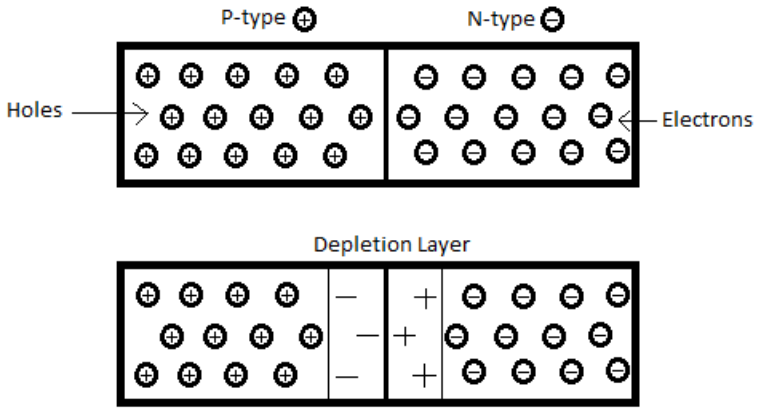

Figure 1 - The above picture depicts a PN junction, and the effect that diffusion and recombination has on the junction, forming a depletion layer. The charges in the depletion region (middle) are fixed and represent ionized dopant atoms.

type layer) atoms, and negatively charged acceptor (p-type layer) atoms (Fig. 1). Without free carriers to screen these charges, an electric field develops in what is often called the depletion region. When an electron from the n-type layer diffuses across the p-n junction, it leaves behind a static positive charge (the donor atom). Likewise, when a hole from the p-type layer diffuses across the p-n junction, it leaves behind a static negative charge (the acceptor atom). As the process of diffusion continues, an electric field begins to form from

the buildup of fixed charges. The resulting electric field creates a situation in which holes are forced to travel in one direction and likewise, electrons can only travel in one direction. When light shines on the p-n junction cell, electrons are excited from the valence band to the conduction band in the depletion region. The electric field separates the resulting electron-hole pair, generating a photocurrent in both the conduction and valence bands simultaneously. The maximum amount of voltage/current available for use out of one of these cells is determined by the makeup and composition of the cell and is defined as the Shockley-Queisser limit.

The Shockley-Queisser limit is also known as the detailed balance limit. It was first calculated by William Shockley and Hans Queisser at Shockley Semiconductor in 1961 [7]. Basically, the detailed balance limit is a fundamental limit that describes the

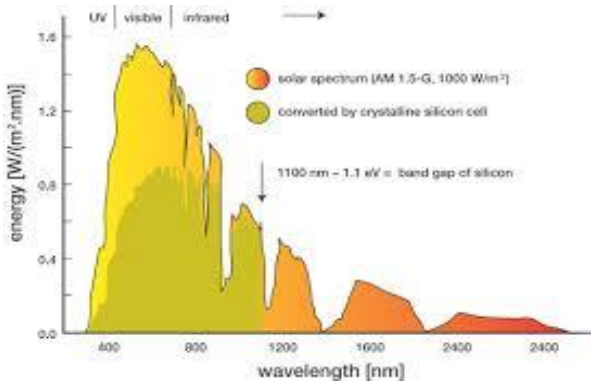

Figure 2 - Depiction of the composition of sun's rays at different wavelengths. As shown above, the majority of the sun's rays reside in the spectrum at a band gap of ~1.5 eV. Figure from Ref. [6].

maximum solar conversion efficiency possible for a single pn junction solar cell. Under the AM1.5g solar spectrum, the limit falls somewhere around 33.7%, corresponding to a single pn junction with a band gap of 1.34 eV [7]. However, the maximum efficiency is rather broad in terms of band gap, so that even a band gap of 1.4-1.5 eV would be equally useful. It might make sense that one would want a small band gap so that all of the energy

from the sun is absorbed. However, most of the energy would be wasted because the energy that actually goes towards a load is the energy obtained in the transition from the valence band to the conduction band. On the other hand, if the band gap is too large, very little of the solar spectrum would be absorbed by the solar cell. For this reason the ideal band gap varies with the nature of the incident spectrum.

Silicon, however, has a band gap of only 1.1 eV, and hence is not necessarily optimal for terrestrial photovoltaics. It also has what is termed an indirect band gap, meaning the lowest energy point in the conduction band and the highest energy point in the valence band do not align in terms of momentum. This leads to a semiconductor material that it is a relatively poor absorber of light, as a lattice vibration, or phonon, is needed to conserve momentum. Direct gap materials such as GaAs and InGaAs are better performers, have roughly one order of magnitude greater absorption coefficient, and also have a band gap that is a closer match to the solar spectrum. Unfortunately, gallium and indium are somewhat scarce, creating concerns about long term supply. Because of this, there is considerable interest in so-called "earth abundant element" alternatives with direct band gaps appropriate for photovoltaic devices. There are a number of candidates currently being explored. The subject of this thesis is $ZnSnN_2$, one such candidate comprised of only earth-abundant elements.

Interest in this material arose because in addition to being earth abundant, zinc and tin also benefit from a very mature recycling infrastructure. Because there are ways to recycle the materials to be "as new," there is less worry about what happens when the material is at the end of its lifetime; no questions wondering how to get rid of the material as you can recycle it and use it for other applications if not to be used in the creation of

more thin film semiconductors. All of this adds to the promise of $ZnSnN_2$ which may prove to be a viable replacement for indium or gallium based semiconductors. $ZnSnN_2$ is also desirable because it shows evidence of band gap tuneability between 1 eV and 2 eV, allowing for the thin film to hit the maximum efficiency for an earthbound solar cell at 1.5 eV [8], as described earlier by the Shockley Quiessar limit. It is worth noting that $ZnSnN_2$ is not all that distant in terms of the location of its constituent elements from InGaN (Fig. 3).

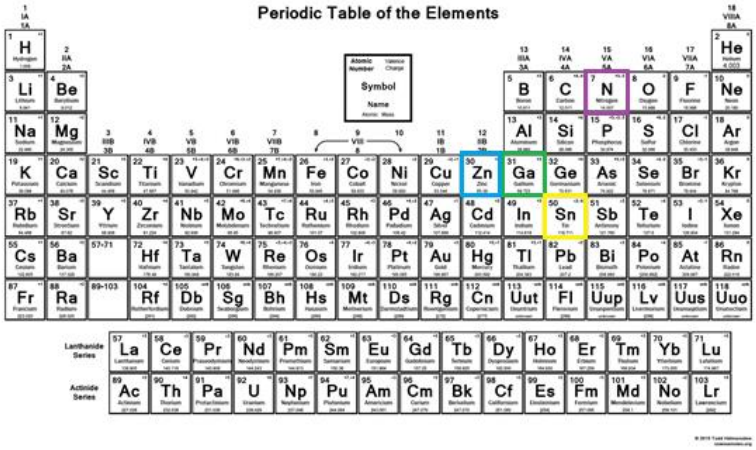

Figure 3 - The periodic table of elements. Highlighted is the III-V semiconductor, GaN and the earth abundant elements, Zinc and Tin, that will be used to convert this III-V semiconductor into a II-IV-V semiconductor.

1.2 Ternary Heterovalent Compounds

The concept of a ternary heterovalent compound is not new. Goodman reported a study of several close analogs to conventional III-V semiconductors (for example, GaAs) in 1957 [Nature 1957]. The concept is that pairs of the column III element are replaced by

a pair of atoms, one from column II (such as Zn or Cd) and one from column IV (for example, Si, or Sn). The result is a stoichiometric compound of the formula II-IV-V_2. In a similar fashion, the commercially important solar cell material copper indium gallium disulfide ("CIGS") is based on a I-III-VI_2 compound, and directly analogous to the II-VI compounds (for example, CdTe or ZnSe). Goodman, however, did not consider the nitrides, which had to wait until 2005 when Lambrecht's group studied the structure and phonons of $ZnGeN_2$ [9].

1.3 $ZnSnN_2$

$Zn-IV-N_2$ was first described by Tula R. Paudel and Walter R. L. Lambrecht in their 2008 paper "First-principles study of phonons and related ground-state properties and spectra in $Zn-IV-N_2$ compounds" [10]. In this paper, the correlation between periodic table proximity and band gap, structure, and carrier density is studied with a main focus on spectra. Reports include information on structural and elastic properties such as the lattice constants and bulk moduli. Calculations of the phonons and such related quantities are estimated using density-functional perturbation theory in the local-density approximation and using a plane-wave pseudopotential method. [10]

Veal et al. described the first single crystal growth of *$ZnSnN_2$*, using the same MBE system as in the present study. They also presented DFT calculations for both the fully ordered orthorhombic lattice, with a predicted band gap energy of 2.0 eV, and a model for a completely randomized Zn and Sn sublattice in a monoclinic/wurtzitic lattice, which

yielded a predicted band gap of 1.0 eV. [11] Thus, the "ideal" band gap energy of 1.5 eV for a terrestrial solar cell would lie half-way between these two extreme cases.

The Atwater group at the California Institute of Technology reported successful growth of $ZnSnN_2$ the same year, using the technique of RF sputtering instead [12]. This technique yielded high-quality, although polycrystalline, thin films. Subsequent predictions by the same group suggested a slightly different band gap energy of 1.42 eV [12]. The group of Kathleen Kash at Case Western Reserve has also grown $ZnSnN_2$, using a vapor-liquid-solid (VLS) growth process, which yields micron sized needles which are difficult to characterize [13]. The same group recently investigated lattice ordering phenomena for heterovalent ternaries. Results pertaining to $ZnSnN_2$ have been published and it has been suggested that the orthorhombic lattice structure is too thermodynamically unfavorable to occur during growth. [14] Several other groups have also reported growth and characterization of $ZnSnN_2$. Lahourcade et al. have reported experimental optical gaps in the range of 1.9 to 2.2 eV (sputtered thin films, $n \sim 10^{21}$ cm^{-3}) [12]. Quayle et al. reported broad photoluminescence between 1.4 and 1.6 eV, and a photoluminescence excitation spectroscopy estimated gap of 1.7 eV. (VLS, n unknown). Deng reported estimated gaps in the range of 1.82 eV to 1.95 eV, with significant absorption above 1.4 eV ($n \sim 10^{17}$-10^{18} cm^{-3}). Fioretti et al. have reported absorption onsets in the range of 1.0 to 1.4 eV ($n \sim 10^{18}$-10^{20} cm^{-3}). Recently, Qualye et al. proposed an alternative perspective on disorder, arguing that the octet rule should dictate the details of atomic ordering, and predict a band gap energy relatively insensitive to cation sublattice disorder. [15]

1.4 Overview of Thesis

This thesis is a study that analyzes the plasma-assisted molecular beam epitaxy (MBE) growth of $ZnSnN_2$ thin films, a material of interest for photovoltaic device applications, with a view towards achieving improved cation (Zn and Sn atom) sublattice ordering. The interest in cation ordering stems from recent predictions of the potential for variation of the band gap energy [10]. Growth conditions were varied, and film growth was monitored in-situ using reflection high-energy electron diffraction (RHEED). RHEED patterns were analyzed both in terms of streak width and streak spacing as a function of growth parameters.

Chapter one presents an introduction to photovoltaics and the motivation for choosing $ZnSnN_2$. Chapter Two introduces the reader to a review on the techniques and tools needed for a thorough study on the $ZnSnN_2$ films. Chapter Three presents the results obtained from the film growth experiments, the analyses performed, and the trends observed. Chapter Four provides a brief summary, key conclusions, and insight into the next logical steps for future direction in the study of $ZnSnN_2$.

Chapter 2 Material Synthesis and Characterization

2.1 Molecular Beam Epitaxy

There are many techniques for creating semiconductor crystals, especially in the case of thin films (i.e. less than 10 microns thickness) needed for most device applications. Among the most common are sputtering, chemical vapor deposition, physical vapor deposition, and molecular beam epitaxy (MBE). Differences among them include growth rate, crystal purity, crystal stoichiometry (in the case of compounds), and achievable crystal quality.

The specific technique employed in this thesis to grow the high quality single crystals being sought after is a variation of MBE known as plasma-assisted MBE (or sometimes PAMBE). MBE was invented in the late 1960s at Bell Telephone Laboratories by Al Cho [16]. It is essentially a thermal evaporation process with very low growth rates (controllable to atomic thicknesses), which requires ultra-high vacuum (below 10^{-8} torr, with atmospheric pressure being approximately 720 torr) to maintain semiconductor device-quality purity. It is well-known as a technique capable of growing both single-element (e.g. Si) and compound (e.g. GaAs) single crystal films, almost always by carefully choosing a single crystal template (or substrate). Under the right conditions, the thin film will follow the atomic ordering of the substrate, a process known as epitaxy. If the thin film and substrate are the same material, it is known as homoepitaxy; all other situations are referred to as heteroepitaxy.

A schematic of a typical MBE system is shown in Fig. 4. Key elements are effusion cells used for thermal evaporation; a pumping system used to achieve ultra-high

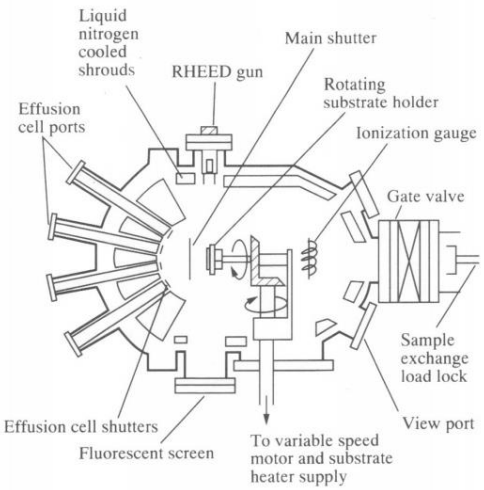

Figure 4 – This figure shows the chamber portion of the MBE machine. As shown, the material sources are setup in such a way as to allow each of their respective fluxes to have minimum interference with each other as well as to equally affect the substrate to be grown on. This setup allows for slow controlled precise growth. Figure from reference [17]

vacuum conditions; a sample/substrate heater; a plasma source or other means of activating molecular gas species such as oxygen or nitrogen (optional); and diagnostic equipment such as residual gas analyzers, reflection high-energy electron diffraction (RHEED), and flux measurement using an ion gauge or quartz crystal microbalance. The instrument of choice to achieve such low pressures in the MBE machine is called a cryopump. A cryopump works by delivering helium gas at approximately 15 K to a manifold exposed to the interior of the MBE system. Gas species condense on this manifold, which must be periodically warmed and purged. A cryopump cannot be started until the pressure is below 10 millitorr, so initial pumping after venting to atmosphere is accomplished with a separate pump. A second pump, referred to as an ion pump, is used in conjunction with the cryopump to maintain ultra-high vacuum conditions. This pump employs a hot filament to

generate electrons. These electrons ionize gas atoms, which are then accelerated by an electric field, and subsequently implanted into titanium plates. Periodically it is necessary to replace the plates as a result.

2.2 Flux Measurement

An effusion cell used in MBE applications is basically a crucible, often made from pyrolytic boron nitride, with a capacity of approximately 40-100 cc; smaller volumes are used for dopant or specialty sources. The crucible is heated to the temperature necessary to obtain the desired atomic/molecular flux, or arrival rate per unit area. Temperature is monitored by a thermocouple, and maintained using a proportional-integral-derivative (PID) controller in closed loop. Flux is measured in the current system using a quartz crystal microbalance, or QCM, which is mounted on a bellows assembly to allow it to be positioned where the substrate usually lies. The flux determines the growth rate, as well as stoichiometry and crystal quality, and so is an important parameter. Each effusion cell has a pneumatic shutter which can block the flux when needed.

A QCM works through the use of a piezoelectric quartz crystal which collects matter on its surface, changing its resonant frequency (typically near 6 MHz). The unit employed in this work has its own pneumatic shutter to prevent material accumulation during growth. Knowledge of the mass of the arriving species, coupled with measuring the frequency change with a frequency counter, allows the flux (atoms/cm^{2}·s) to be measured.

Unloaded, the QCM operates at approximately 6 MHz. The measured frequency then starts to decrease as material is deposited on it. The frequency difference (Δf) is sampled every 5 seconds and corresponds to a particular flux value (Γ).

The equation to obtain the flux is:

$$\Gamma = \frac{\frac{\Delta f * \sqrt{\Phi q * D q *}\, \pi * d}{2 * F_0^2 * t} * N_A}{M} \qquad (1)$$

where Δf is the crystal frequency change (Hz), Φ_q is the shear modulus of quartz ($2.95 * 10^{11}\ g{\cdot}cm^{-1} * s^{-2}$), D_q is the density of the quartz ($2.648\ g{\cdot}cm^{-3}$), d is the diameter of the quartz (0.5 cm), F_0 is the frequency of the clean crystal (6 MHz), t is the sample time (5 s), N_A is Avogadro's number ($6.02 * 10^{23}\ molecules{\cdot}mol^{-1}$), and M is the molecular weight of the measured deposited material (g*mol^{-1}). The starting point, however, is usually a theoretical flux obtained from the Knudsen equation:

$$\Gamma_e = \frac{dN_e}{dt} = A_e p_{eq} \sqrt{\frac{N_A}{2\pi M k_B T}} \qquad (2)$$

where Γ_e is the total effusion rate, A_e is the surface area of the evaporating material, p_{eq} is the equilibrium pressure of the material at a temperature T, M is the molecular weight of the evaporating species and N_A and $k_B T$ are Avogadro's number and the Boltzmann constant, respectively. The vapor pressure equivalent is typically obtained from published

curves, such as those in ref [18]. Theoretical curves for both Sn and Zn are shown in Fig. 5.

It should be noted that experimental curves typically do not match the predicted curves exactly. This is due to several factors; when creating our curves, we made assumptions

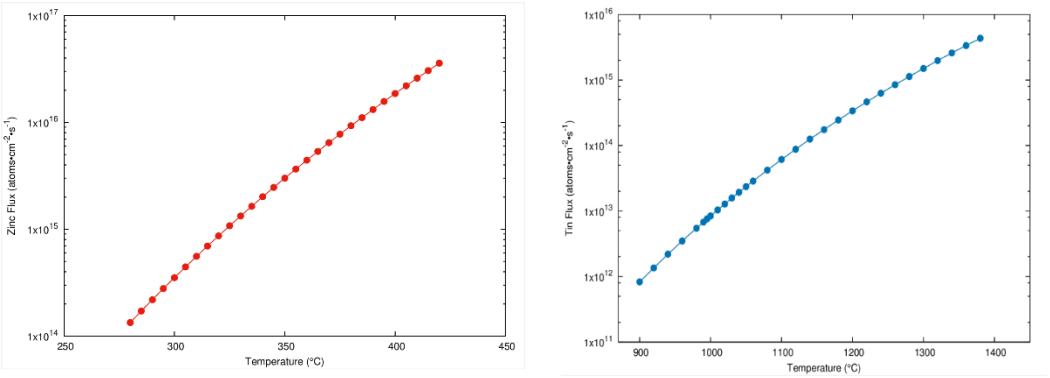

Figure 5 – 60 cc Zinc (left) and 30 cc Tin (right) calculated flux curves.

about the cells and vapor pressure. We assumed a perfect Knudsen cell even though our cells might not be perfect Knudsen cells. The distribution of the material within the crucible could also be different depending on temperature- could be liquid or solid. The angle at which the source makes with the crystal monitor/sample isn't perfect either. The shape of the crucible might also not be optimal. Thus, the procedure is to select a flux based on desired growth conditions and growth rate, use the theoretical curve to estimate an effusion cell temperature, and then measure the actual flux with the QCM. The theoretical curve can be used to estimate the necessary temperature change if the desired flux is not achieved, by scaling it with an experimental data point.

2.3 Active Nitrogen

Nitrogen is a molecular gas (N_2) at room temperature, and relatively inert. To ensure it reacts with the zinc and tin atoms also arriving at the substrate surface, some type of "active" nitrogen is needed. For MBE, ammonia can be used, but only at elevated temperatures needed to crack it into atomic species. An alternative is a plasma source. Two main types in common use are the electron cyclotron resonance (ECR) microwave source, and the radio frequency (RF) source. Most of the initial work on PAMBE was done using ECR sources [19]. However, most current MBE systems growing nitride semiconductors employ an RF source.

The ECR source operates at a frequency of 2.45 GHz. This high frequency allows the plasma to be confined to a small volume. When nitrogen is introduced to the system, plasma is created in the ECR tube. Because the plasma source and the chamber are directly connected, an aperture plate and a pyrolytic boron nitride liner are introduced in order to minimize contamination from sputtering of the source walls [19]. In contrast, the RF source operates at a frequency of 13.56 MHz with a maximum power of 600 watts. To minimize contamination, the discharge is electrodeless. It appears that the ECR source may provide a better degree of cracking into atomic species (e.g. $N_2 \rightarrow 2N$), whereas the RF source provides excited molecular species (e.g. N_2^*), especially at lower powers. The best nitrides appear to be achieved at very low power, using an RF source [19]. In the Perkin Elmer model 430 MBE system employed in this work, an Oxford HD25 inductively coupled RF plasma source was installed to provide active nitrogen species.

2.4 Reflection High-Energy Electron Diffraction

One of the most powerful tools in MBE is the ease with which in-situ diagnostics can be integrated. By far, the most popular is reflection high-energy electron diffraction (RHEED). Just like the name implies, RHEED uses high energy electrons in both

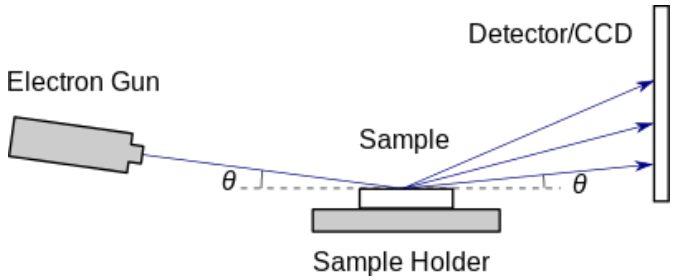

Figure 6 - Here is a depiction of the basic setup of the RHEED system, which is composed of an electron gun, a sample, and a detector.

reflection and diffraction to characterize the crystal surface. A RHEED system requires a number of components (see Fig. 6). At its most basic level, an electron source, or gun, a sample with a clean surface, a sample dock/tray, and a phosphor screen are required. In most systems, the image from the phosphor screen is captured using a CCD camera. The electron beam is incident at a very shallow angle θ, typically less than 1°, which means that fluxes directed at the surface are not blocked by the RHEED system. Electrons are emitted by a heated filament, and accelerated using a potential of 10 – 20 kV. The resulting electron wavelength is given by

$$\lambda = \sqrt{\frac{150.4}{E\ (in\ eV)}}\ in\ \text{Å} \qquad (3)$$

where E is the electron energy, 20 keV in our case. This results in a wavelength λ on the order of 0.0867 Angstroms. Since the atomic spacing is roughly 0.5 nm, it is possible to observe a diffraction pattern from a periodic surface such as that provided by a crystal

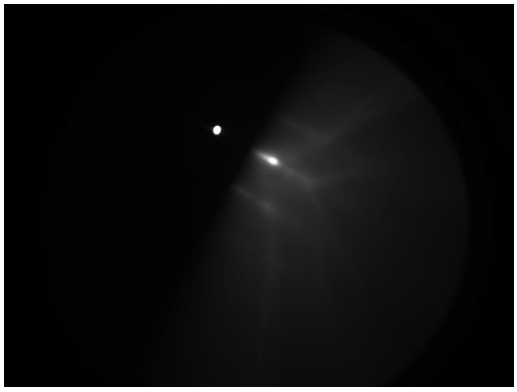

Figure 7 – Typical RHEED pattern of a Yttria-stabilized zirconia (YSZ)(111) substrate. The faint diagonal streaks derive from secondary scattering events called Kikuchi scattering, and are an indication of a very high quality bulk crystal.

substrate or epitaxial thin film. A typical RHEED pattern from a YSZ(111) substrate is shown in Fig. 7. The fact that streaks are obtained from a single crystal stems from constructive and destructive interference due to satisfied Bragg diffraction conditions. A crystal is basically a lattice of points of symmetry where the points are atoms of different elements. In order to obtain constructive interference, the conditions to be met for constructive interference must be met in both real and momentum space.

The streak spacing is inversely proportional to the lattice spacing along the crystalline direction being probed by the electron beam (rotating the crystal allows other

directions to be observed). Due to the shallow incident angle, only a few atomic layers are typically probed by this technique, and if the top surface atoms are periodically arranged, but in a different fashion than the rest of the layer (due to dangling bonds, for example), they may also be probed. The width of the streaks is also an indication of crystal quality, with narrower streaks representing higher crystal quality [20].

2.5 Stoichiometry Determination

A high-quality semiconductor material will generally be stoichiometric to better than 1%. In this work, stoichiometry was verified for select films using the technique of Rutherford backscattering spectrometry (RBS). RBS is a self-standardized technique that was first developed, and named after, Professor Sir Earnest Rutherford. RBS in its early stages was first discovered when Rutherford and his colleagues were attempting to eliminate stray alpha particles from their alpha source while conducting experiments intended to measure alpha particle deflection on its way through gold foil [21]. At that time, the contemporary atomic model was what is termed the “plum pudding” model, which was a model proposed by JJ Thomson in 1904. In this model, JJ Thomson claims that the atom is essentially a cloud of positive charge with points of negative charge placed randomly inside, resulting in an object that is really just open space with particle interactions due to small size of electrons and protons. Based on this model, Rutherford expected to see most of the alpha particles going through the gold foil to pass straight through, or alter their angles slightly based on the occasional particle to particle interaction. However, the transmission results that were obtained were slightly lower than what was expected. In an attempt to see what was going wrong, Rutherford had the alpha particle

sensor moved to the other side of the gold foil to see how many particles were bouncing backwards. The surprising result showed that a fair number of alpha particles were scattering back towards the sensor [21], which was inconsistent with the current model, and led to our present understanding of electron “orbits” around a positively charged nucleus.

In the basic RBS technique, helium ions are emitted from a source and accelerated to an energy of several million electron volts, then directed to the sample to be measured. The desired collision that occurs is called an elastic collision, that is, an interaction in which no energy is lost. After colliding with the nucleus, a few of the particles are scattered backwards in different directions. A select few of these that happen to rebound in the direction of the sensor, which is positioned at a specific angle, have their energy recorded. The remainder of the particles, the majority, either tunnel through the material or get stuck in the material. Using the data recorded, the mass of the particle in the nucleus that the He atom bounced off of can be determined. The results of an example RBS experiment is shown in Fig. 8. You can simulate the spectrum to determine your film composition using SIMNRA, a program designed to simulate and fit RBS spectrum in order to determine the ratio of Zn:Sn or any other ratio. This particular film was grown on a glassy carbon substrate in order to identify the nitrogen peak during RBS. This is due to the fact that the YSZ(111) substrate proves problematic during RBS because it contains oxygen, and the nitrogen peak from the film sits on top of the oxygen peak from the substrate, so we are unable to clearly identify the nitrogen peak. The accuracy of the stoichiometry determination is approximately 1-3% under optimized conditions [23].

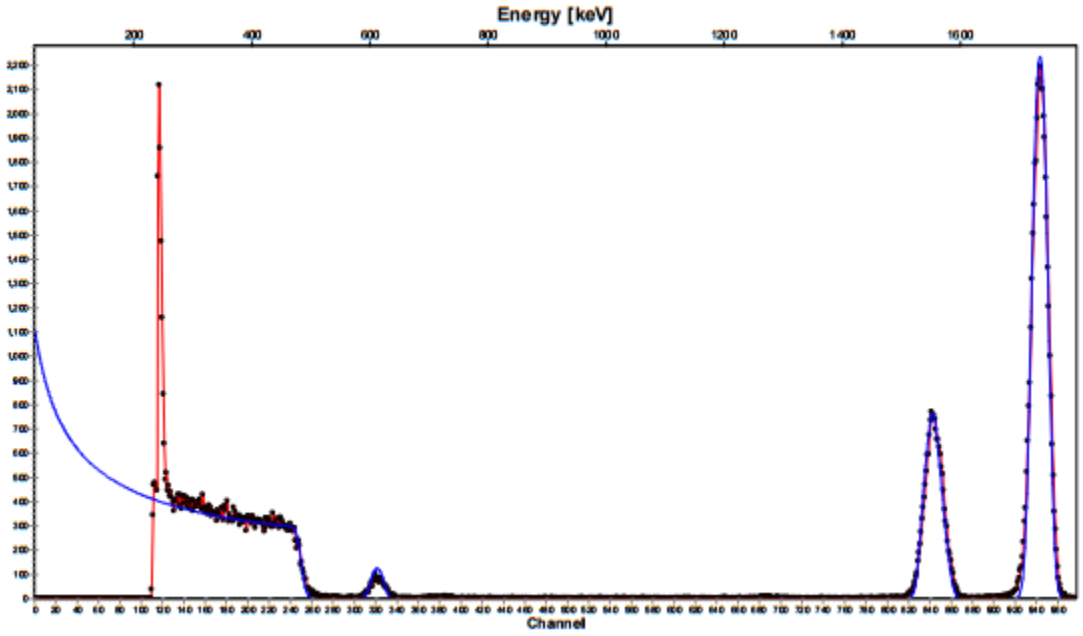

Figure 8 - A chart showing the results for RBS taken on a $ZnSnN_2$ sample at the Department of Physics at Western Michigan University. Depicted are counts versus energy. The peaks from left to right are glassy carbon substrate, nitrogen, zinc, and tin.

2.6 Summary of Previous Growth Experiments

The present work follows after the doctoral studies of Nathaniel Feldberg [22] at the University at Buffalo, who employed the same MBE system prior to its relocation to WMU. In his time at University at Buffalo, Feldberg studied $ZnSnN_2$. From his studies, it was shown that $ZnSnN_2$ could be successfully tuned from polycrystalline to single crystalline. He specifically found that the controlling factor was the ratio of the zinc flux to the tin flux. An overpressure of zinc flux was necessary in order to achieve single crystalline growth. Even though theoretically predicted to grow in the orthorhombic

structure, $ZnSnN_2$ was grown wurzitic every time and characterized using electron microscopy, x-ray and electron diffraction, x-ray photoelectron techniques and optical absorption. Many of the films were degenerately n-type doped, a trait that could be attributed to native defects in the crystal. To aid in this, YSZ(111) was used because of its small lattice mismatch to $ZnSnN_2$. A crystal that is being grown on a substrate that has a low mismatch is less likely to contain defects as there is less internal strain to deal with during the growth process. Also, YSZ(111) is an oxide and doesn't have to deal with the problems inherent to many experiments which involve problems dealing with oxide layers (which are typically amorphous, nonstoichiometric, and must be thermally or chemically removed prior to using the substrate). Much of the analysis done in this work is done using the films that Feldberg grew.

3.1 Introduction

Prior to the beginning of this work, characterization of the films was focused on using x-ray diffraction, scanning electron microscopy, Hall effect measurements and optical absorption spectroscopy. Only two films – among the very last ones grown at the University at Buffalo – showed any indication of orthorhombic crystal structure using syncatronion radiation x-ray diffraction (which was performed after growth, ex-situ, by collaborators at other institutions). RHEED was employed largely as a qualitative tool, although quantitative information is possible, and is the focus of the present work.

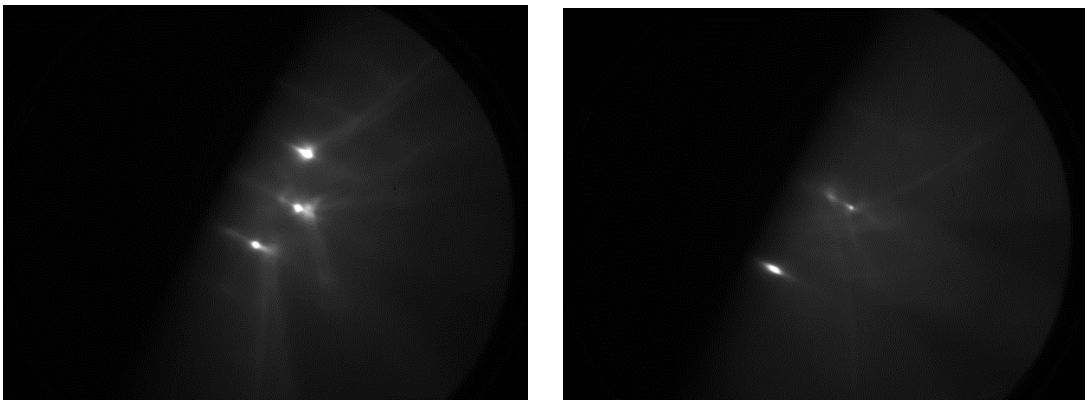

Figure 9 – a) RHEED streaks of a substrate oriented at 0 degrees before growth. (left picture) b) RHEED streaks of a substrate rotated 30 degrees from (a) (right picture)

Fig. 9a is a picture of one typical RHEED pattern when a RHEED acquisition is performed on a YSZ(111) substrate, which is the substrate employed in this study. The second image, shown in Fig. 9b, is the same substrate after it is rotated 30 degrees.

Although YSZ is a cubic crystal, the symmetry of the (111) planar surface is hexagonal; one should expect the patterns to repeat every 60 degrees.

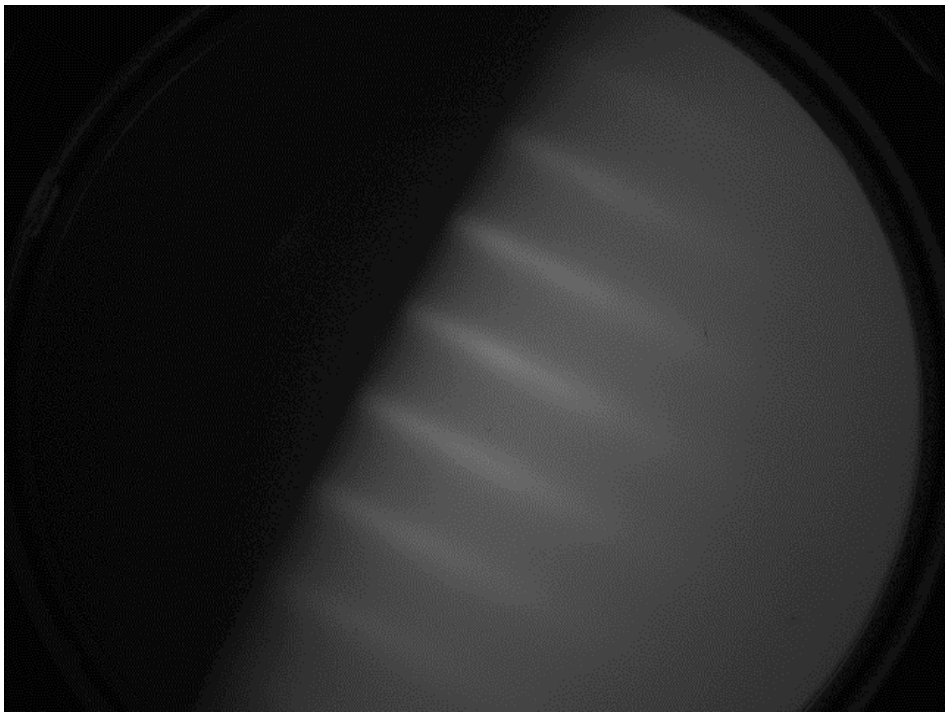

Figure 10 - RHEED streaks showing a crystal lattice after a one hour growth. Notice the doubling of the number of streaks when compared to a substrate RHEED pattern.

The films being analyzed are the substrates being grown on and the one hour growth RHEED patterns with the exception of one or two films. We expect most of our one hour growth experiments to result in a RHEED image like that of Fig. 10. A single crystal film exhibits parallel streaks. Due to a rough surface (on an atomic scale) and a lack of perfect crystallinity, the stress in general will be somewhat indistinct.

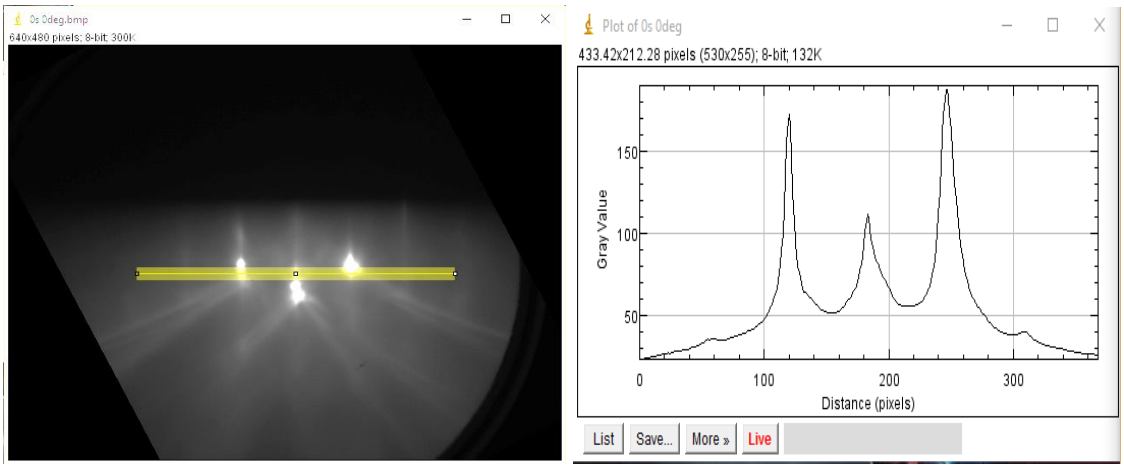

Figure 11 - Line profile running across regions of high and low intensity on a RHEED pattern in ImageJ (left picture). Resulting graph of the line profile showing a curve (with resulting data points) for the RHEED line profiling using ImageJ (right).

3.2 Analysis

In order to analyze the RHEED data, a program called ImageJ was employed. ImageJ provides the capability to measure intensities of streaks using a line profile through a graph of pixel versus intensity as shown in Fig. 11**.** First, a line profile is performed on the substrate, rotated to have the line profile facing upwards just for simplicity. The substrate is measured first to provide a reference point that can be used later to create a conversion factor since the lattice constant is known. A typical film RHEED pattern will have at least three clear streaks: the (00),(01), and (01') features.

Since the diffraction pattern is a fourier transform, similar to what a glass lens achieves with optical wavelengths, the streak spacing is inversely proportional to the actual atomic spacing along the crystalline direction being viewed. Knowledge of the substrate lattice constant allows us to compute the film lattice constant.

For the analysis which follows, a program was employed which fits the raw data curves such as those in Fig. 11 to a specified number of Gaussians depending on the pattern obtained. For example, in the case of Fig. 11, four Gaussians were employed, where three of the Gaussians are the primary peaks shown and one Gaussian accounts for the background. In the event that a particular image could not be accurately processed, usually due to weak or no peaks recognizable by the program, a hand analysis is performed..

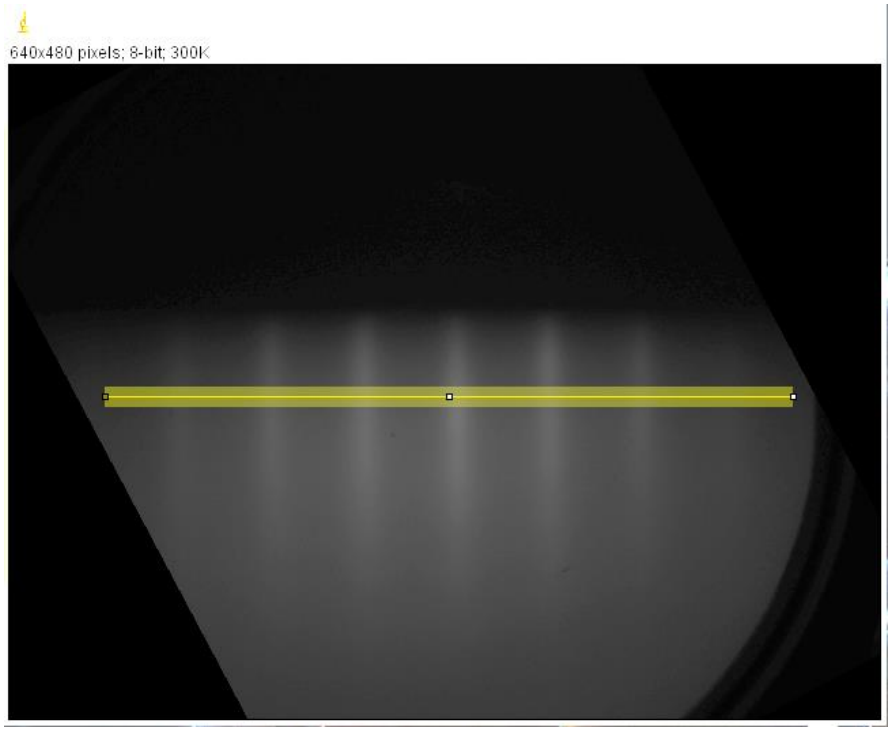

Figure 12 - RHEED streak ImageJ line profiling of 1hour growth. Notice the results showing more gaussians due to the doubling of streaks during growth.

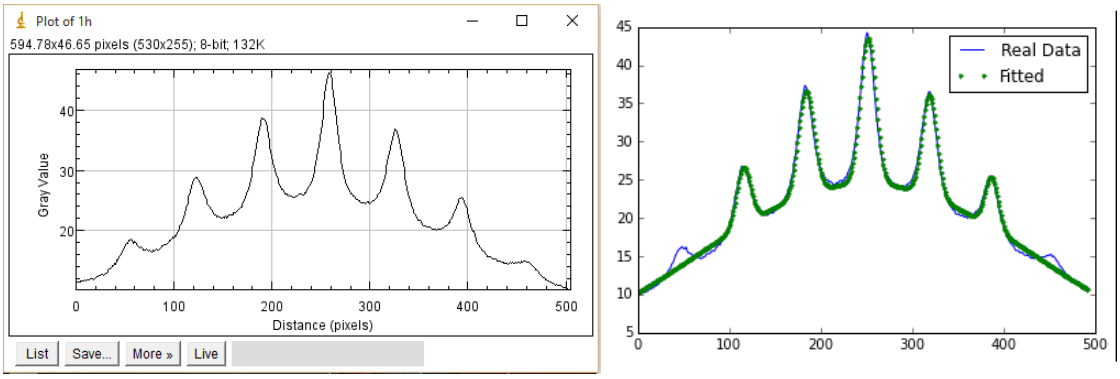

Figure 13 - Line profile obtained from ImageJ (left) and Line profile fit to program written to analyze the profiles obtained (right).

To compute the atomic spacing (a) along the specific crystal direction, we can employ the relation:

$$a = \frac{L\lambda}{t} \tag{4}$$

where L is the distance from the camera to the screen, t is the spacing in pixels between adjacent RHEED streaks, and λ is the wavelength of the electron beam. However, determining L and λ accurately enough is problematic, so we take a ratio of the lattice constant for the substrate over the lattice constant for the film instead:

$$a_{film} = \frac{t_{substrate}}{t_{film}} * a_{substrate} \tag{5}$$

In terms of crystal quality, the full-width at half-maximum (FWHM) is a useful quantitative measure. Given the fact that the film had been grown over a range of

parameter values, we can compare how the FWHM varies as a function of metal to nitrogen ratio, growth temperature, and Zn:Sn ratio. The narrower the FWHM, the higher quality the film. The goal is to identify through analysis of the RHEED patterns, trends which could allow us to create near-optimized films. Table 1 shows the parameter space covered in this study. Table 2 shows the initial (substrate) streak spacing, spacing after 1 hour of growth (approximately 100 nm thickness) and FWHM for a selected group of films, along with their growth parameters.

Table 1 – Chart relating temperature to flux based on theoretical flux calculations.

Temp	Zn	Temp	Sn	N2
300	7.16E+14	990	6.70E+12	2.00E-05
310	1.06E+15	995	1.37E+13	1.00E-05
315		1000	1.38E+13	
320	7.95E+14	1030	1.68E+13	
325	8.54E+14	1100	5.39E+13	
295	7.09E+14	1050	1.99E+13	
287	4.11E+14	1040	1.86E+13	
271	1.98E+14			

Table 2 – Chart showing the films for analysis after throwing away films that didn't have sufficient data. Incorporating Table 1, 2, and the Lab summary sheet, we obtained this table.

Film #	0sec 0deg average spacing	1h average spacing	FWHM	Zn:Sn	Zn+Sn:N2	GM (℃)	RF Power (W)
36	63.94	67.79	7.98	35.97	3.68E+19	400	150
47	51.30	55.78	6.85	38.37	3.68E+19	350	150
48	78.47	94.71	8.83	10.65	1.09E+19	350	150
58	51.44	56.70	5.81	106.89	3.62E+19	400	150
60	55.06	59.31	6.41	106.89	3.62E+19	400	150
62	51.13	54.90	5.22	106.89	7.17E+19	400	150
66	54.58	55.34	4.80	127.46	8.61E+19	500	150
67	56.86	61.50	9.18	38.37	3.68E+19	450	150
71	59.40	60.92	6.44	127.46	8.61E+19	550	150

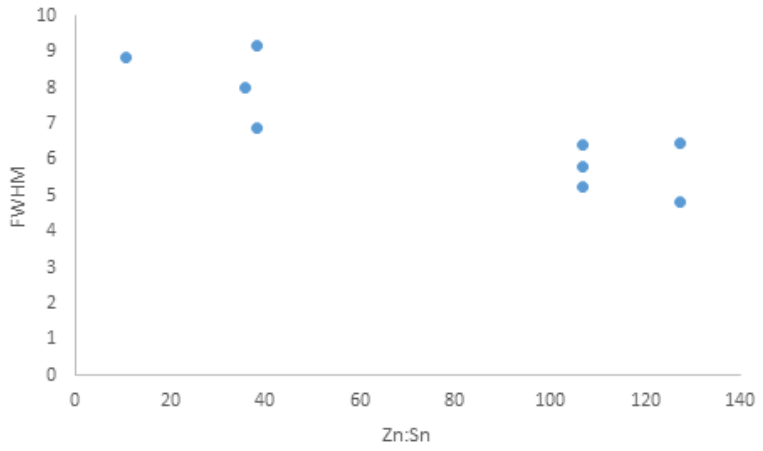

Figure 14 – Chart 1 - Data points obtained from the FWHM vs Zn:Sn graph.

Figure 14 shows the FWHM vs Zn:Sn ratio of a series of films grown. The FWHM varies with the Zn:Sn flux ratio employed. Some scatter is to be expected as other

parameters vary as well. Still, we see a clear improvement in crystal quality as the Zn overpressure is increased.

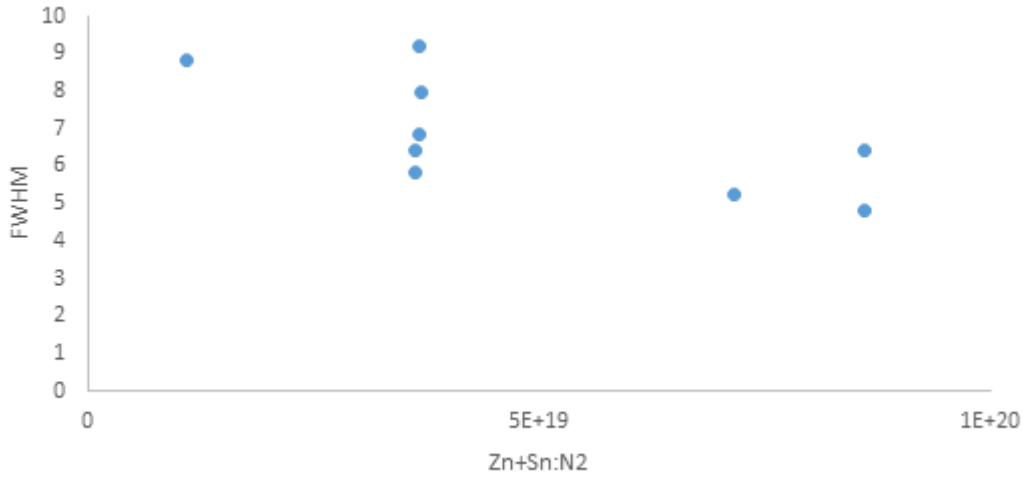

Figure 15 – Chart 2 – Plot of RHEED streak FWHM as a function of total metal (Zn+Sn) flux to nitrogen pressure ratio.

Figure 15 shows the FWHM as a function of the ratio of total metal flux (Zn+Sn) to nitrogen pressure. We make the implicit assumption here that the flux of active nitrogen species is directly proportional to nitrogen pressure. We see a clear trend of reduced FWHM – indicating improved crystal quality- with increasing metal to nitrogen flux ratio.

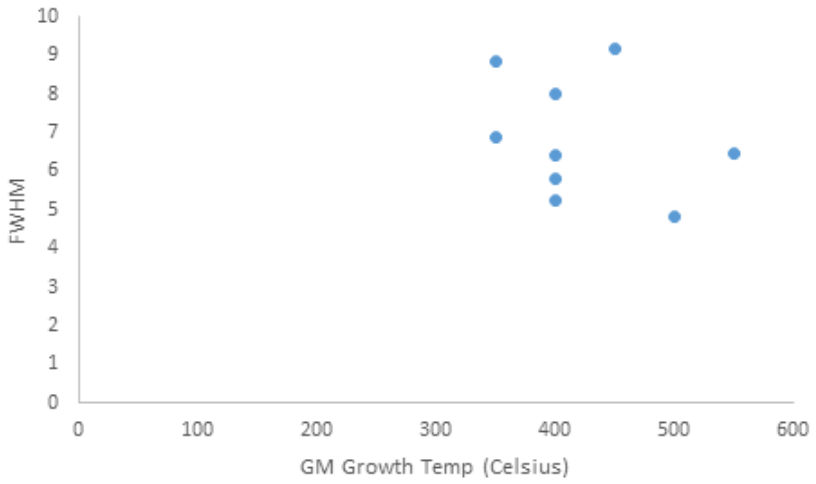

Figure 16 – Chart 3 - Data points obtained from the FWHM vs GM Temperature graph.

In the case of varying the substrate temperatures, we do not see as clear of a trend (Fig. 16). However, it is important to remember that other growth parameters vary somewhat for the films represented in the plot. Ignoring the outlier at 450°C, the trend towards increased crystal quality (decreased RHEED streak FWHM) is apparent.

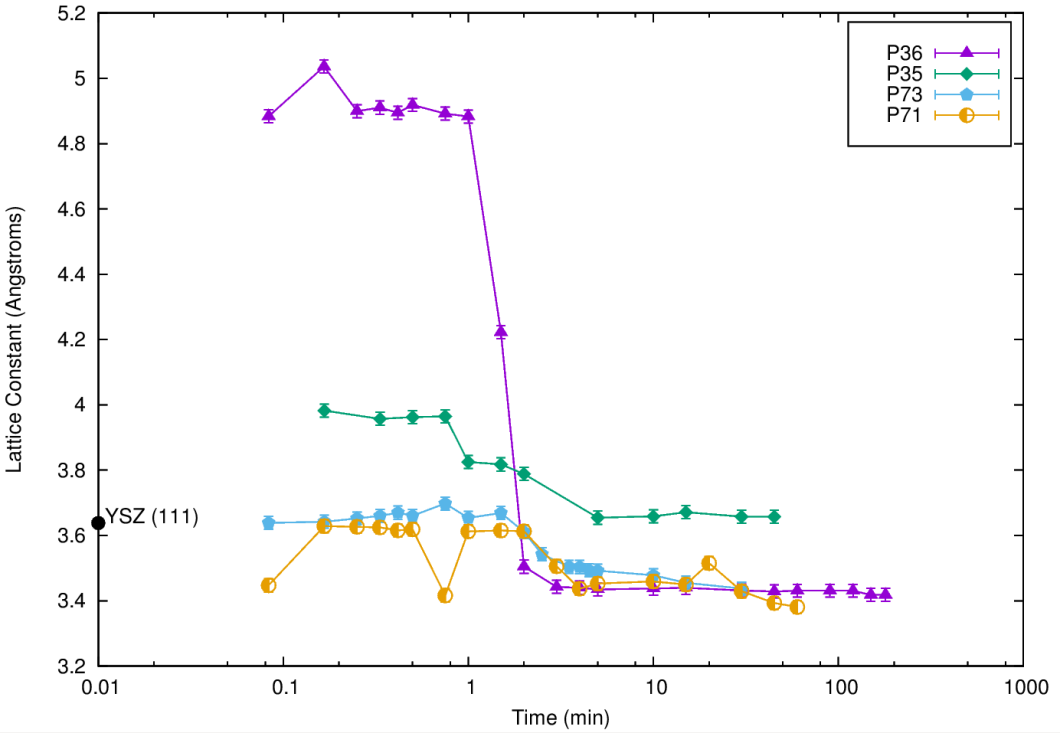

Figure 17 – Extracted lattice spacing for 4 key films as a function of time (corresponding to film thickness)

Another useful parameter that we can extract from the RHEED pattern is the atomic spacing along a specified crystal direction. Using the technique discussed previously in this chapter, we now have a way to monitor lattice constant and thus, the effect of strain on the structure of the crystal being grown. Out of a series of films grown named P35, P36, P71, and P73, shown in Fig. 17 it is seen that P35 and P36, two films with higher initial lattice mismatch (34.14% for P36 and 9.4% for P35) tended toward the wurzitic phase whereas P71 and P73, two films that had a very small lattice mismatch (0% for P73 and 5.25% for P71) tended toward the orthorhombic phase. It can be inferred from this result that initial stress plays an important role on the outcome structure of a crystal.

Using the information gathered thus far, we arrive at a point where we can now form a hypothesis as to how to grow a high quality orthorhombic $ZnSnN_2$ thin film. From the FWHM analysis, it was determined that higher quality $ZnSnN_2$ crystals result from higher Zn:Sn flux ratios; that is, a higher zinc flux than a tin flux, on the order of 10^2. Also, higher quality crystals result from higher metal to nitrogen ratios as depicted by Fig. [15]. The third strong trend that we come across is the lattice mismatch tendencies that we see from films P35, P36, P71, and P73. The two films that exhibit orthorhombic properties, P71 and P73, have a small lattice mismatch to the substrate and lower nitrogen pressures than P35 and P36, two films that exhibited wurtzitic features. P73, which exhibits a 0% lattice mismatch was grown with a lower nitrogen flux. P71, which also exhibits orthorhombic properties, was grown at higher temperature.

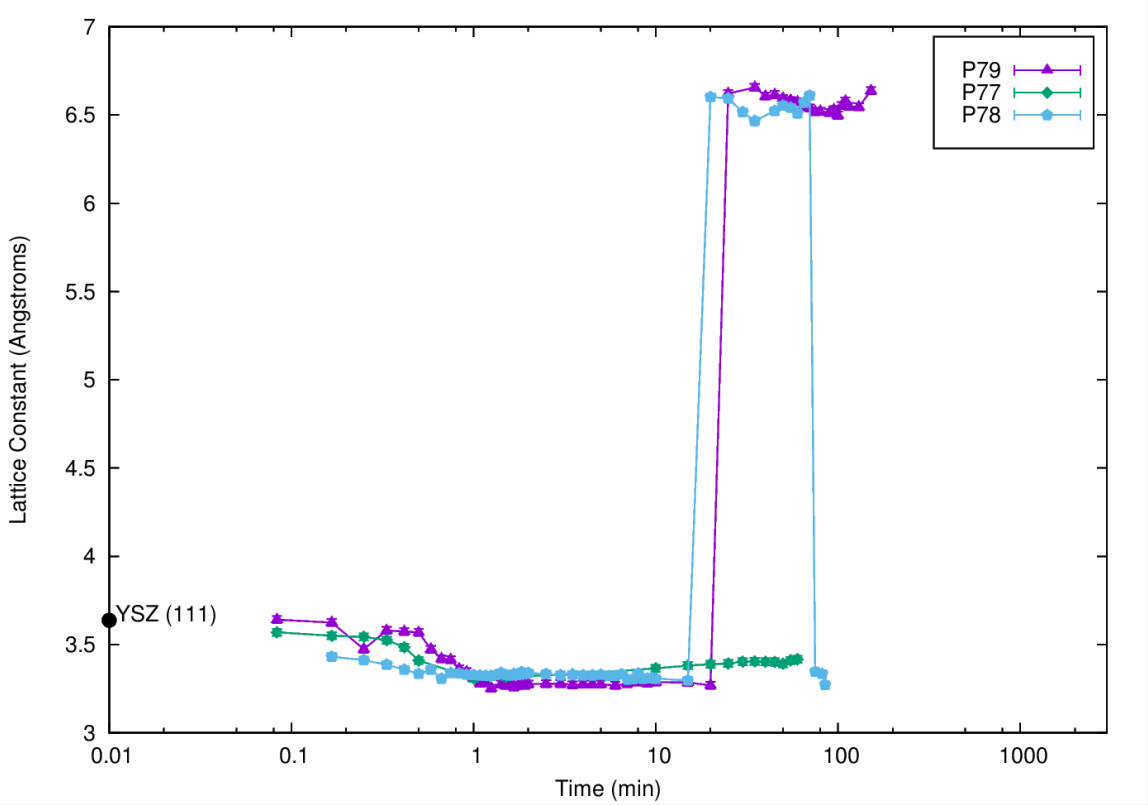

Figure 18 - Lattice Constant vs Time for three recent films grown. Two of the films P78 and P79 exhibit orthorhombic symmetry.

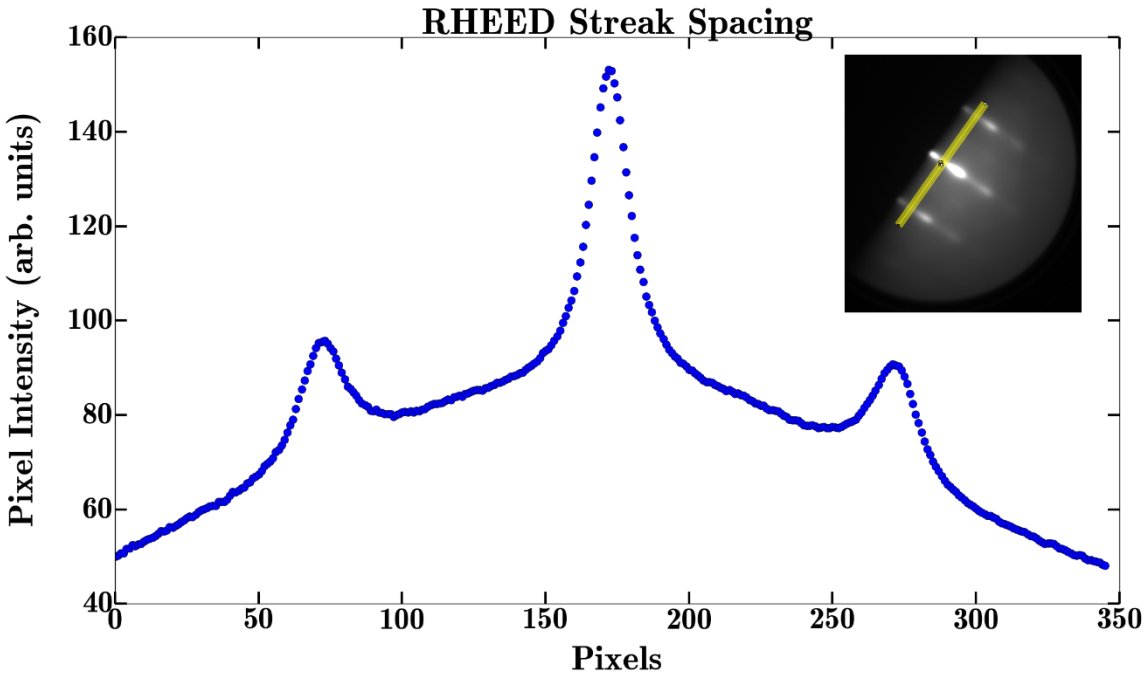

Figure 19 - RHEED pattern depicting single set of streaks.

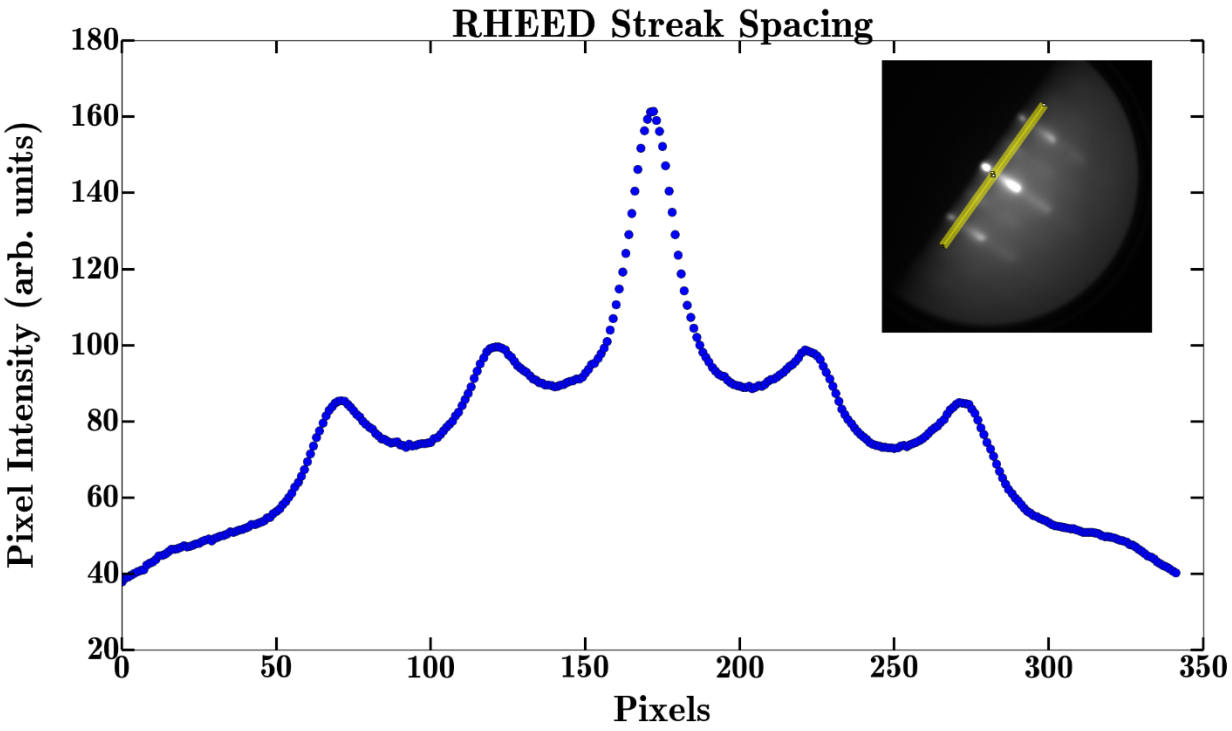

Figure 20 - RHEED pattern depicting the doubling of streaks.

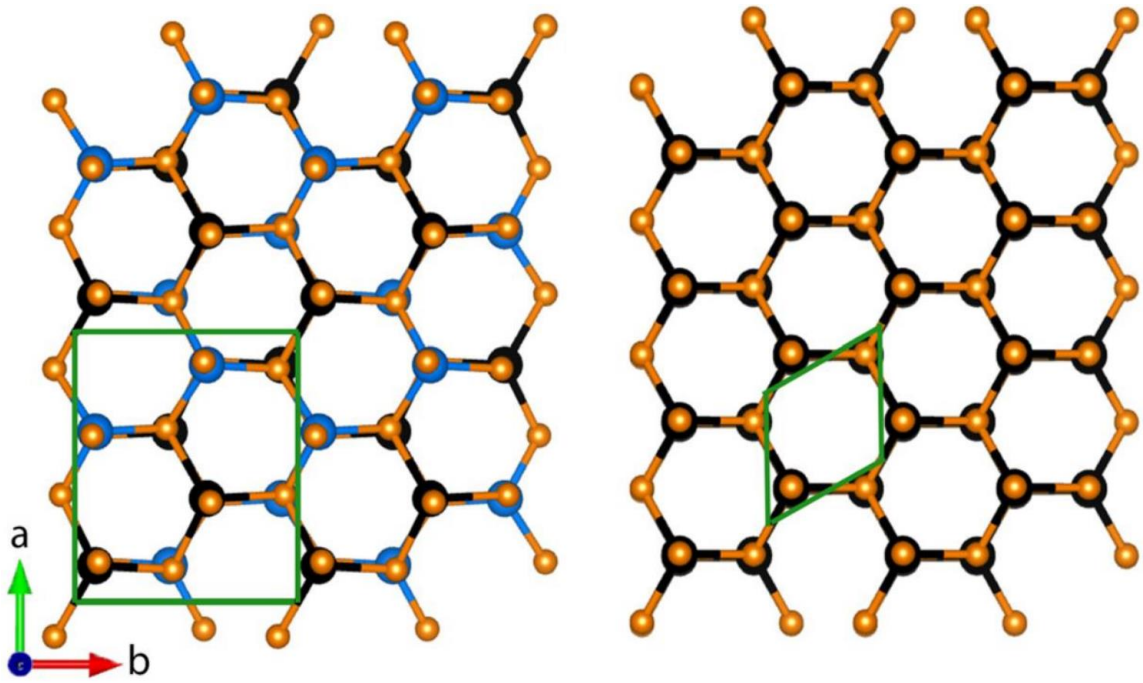

Figure 21 - Unit cell structure of an orthorhombic cell (left) and a wurzitic cell (right). Note the doubling of the atomic spacing from the wurzitic cell to the fully ordered orthorhombic cell.

Figures 19 and 20 show a doubling of the RHEED streaks as expected for orthorhombic growth. Figure 21 illustrates on an atomic scale the transition from a disordered cell (wurzitic), shown on the right, to an ordered cell (orthorhombic), shown on the left. It can be seen that the atomic spacing doubles when transitioning from a disordered cell to an ordered cell. These observations are important when considering what RHEED patterns indicate orthorhombic- like growth.

Based on the results, a series of films was grown which showed signs of orthorhombic growth as can be seen from the doubling of the lattice spacing in films P78 and P79 (see Fig. 18, 19, 20). Unfortunately, miscalculations on P77 lead to a high Sn flux, so orthorhombic growth wasn't achieved. Even though we achieved orthorhombic growth, the films were very thin, so thin in fact that many of the analytical tests that we would normally run on films weren't able to be used. RBS showed that we were growing ultrathin films (thickness ~ $10^{-9}\,m$)(See Fig. 22). Based on previous growth rates, the

expected thickness was approximately 100 times this [Fig. 23]. Subsequent growth experiments resulted in no measurable thickness. This was evident by the fact that throughout the whole growth, we saw Kikuchi patterns and the streak spacing did not change on the RHEED pattern.

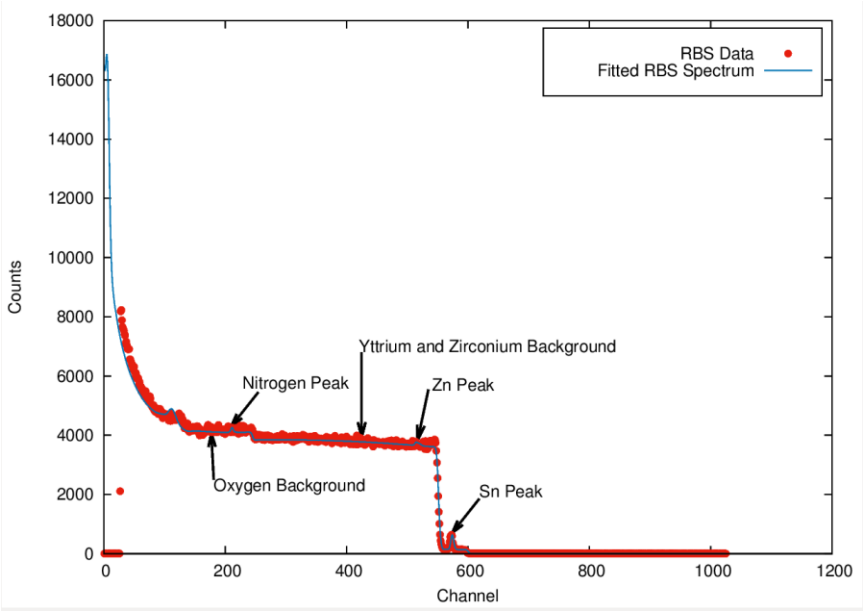

Figure 22 – RBS data depicting an ultrathin film. Notice the lack of intensive peaks at Zn and Sn sites.

We concluded that the holes on the nitrogen source aperture plate had grown shut so that there was no active nitrogen impinging on the film. This, however, supports the

previous work that high metal to nitrogen ratios leads to higher quality, more highly ordered films.

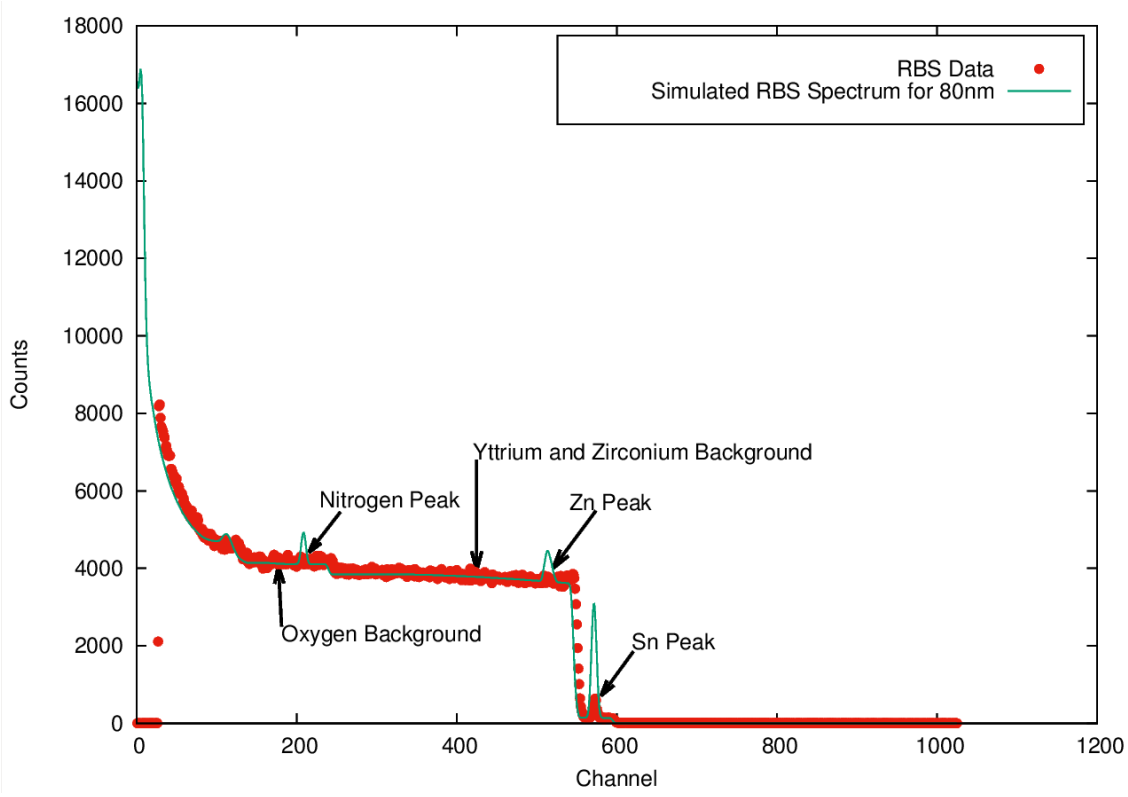

Figure 23 – RBS Data depicting a "stoichiometric" $ZnSnN_2$ film. Notice the pronounced amplitude at Zn and Sn peaks.

Chapter 4 Summary, Conclusions, and Directions for Future Work

4.1 Summary and Conclusions

Based on previous experiments by Feldberg, we saw that high quality films could be obtained by optimizing growth conditions; higher Zn:Sn ratio, higher metal:nitrogen ratio, and higher growth temperatures all yielded higher quality films. We also noted that a lower nitrogen flux and a higher growth temperature led to films that displayed orthorhombic features as well as noting that lattice strain seems to play a role in determining the structure that the film takes.

4.2 Directions for Future Work

For future work, we could first start by attempting to grow orthorhombic films according to our results; Growing in Zinc rich conditions with a higher temperature and lower nitrogen flux theoretically yields higher quality crystals. An interesting direction to take would also be to try to use a different kind of nitrogen source, such as ECR, or try using different parameters for our nitrogen source; if we could produce more atomic nitrogen or excited molecular nitrogen, we might see different results depending on the species of nitrogen used.

Atwater et al. describes adding germanium to $ZnSnN_2$ to open up the band gap a bit. It also allows us to have another degree of freedom in parameter control. [24]

Bibliography

---

[1] Williams, Richard. "Becquerel photovoltaic effect in binary compounds." *The journal of Chemical physics* 32.5 (1960): 1505-1514.

[2] Shaff, J. H. & Ohl, R.S. "Development of silicon crystal rectifiers for microwave radar receivers," *Bell System Technical Journal* Vol. 26 (1947) p. 1

[3] Neville Williams, *Chasing the Sun: Solar Adventures Around the World*, p. 84, New Society Publishers, 2005.

[4] Perlin, John (1999). From space to Earth: the story of solar electricity. Pg. 53

[5] Geoffrey Carr (2012-11-21). "Sunny Uplands: Alternative energy will no longer be alternative". *The Economist*. Retrieved 2012-12-28

[6] "Solar Efficiency Limits" ;http://solarcellcentral.com/limits_page.html/ [Accessed November 15, 2015]

[7] William Shockley and Hans J. Queisser, "Detailed Balance Limit of Efficiency of p-n Junction Solar Cells", *Journal of Applied Physics*, Volume 32 (March 1961), pp. 510-519

[8] T.D. Veal, N. Feldberg, N.F. Quackenbush, W.M. Linhart, D.O. Scanlon, L.F.J. Piper, and S.M. Durbin, "Band gap dependence on cation disorder in $ZnSnN_2$," Advanced Energy Materials (2015) online 29 October

[9] Lambrecht, Walter R. L., Erik Alldredge, and Kwiseon Kim. "Structure and Phonons of Zn Ge N 2." *Phys. Rev. B Physical Review B*. Print.

[10] Paudel, Tula R., and Walter R. L. Lambrecht. "First-principles Study of Phonons and Related Ground-state Properties and Spectra in Zn-IV-N 2 Compounds." *Phys. Rev. B Physical Review B*. Print.

[11] Veal, Tim D., Nathaniel Feldberg, Nicholas F. Quackenbush, Wojciech M. Linhart, David O. Scanlon, Louis F. J. Piper, and Steven M. Durbin. "Band Gap Dependence on Cation Disorder in $ZnSnN_2$ Solar Absorber." *Advanced Energy Materials Adv. Energy Mater.* Print.

[12] Lahourcade, Lise, Naomi C. Coronel, Kris T. Delaney, Sujeet K. Shukla, Nicola A. Spaldin, and Harry A. Atwater. "Structural and Optoelectronic Characterization of RF Sputtered $ZnSnN_2$." *Adv. Mater. Advanced Materials* (2013): 2562-566. Print.

[13] Quayle, Paul C., Keliang He, Jie Shan, and Kathleen Kash. "Synthesis, Lattice Structure, and Band Gap of $ZnSnN_2$." *MRC MRS Communications* (2013): 135-38. Print.

[14] Quayle, Paul C., Eric W. Blanton, Atchara Punya, Grant T. Junno, Keliang He, Lu Han, Hongping Zhao, Jie Shan, Walter R. L. Lambrecht, and Kathleen Kash. "Charge-neutral Disorder and Polytypes in Heterovalent Wurtzite-based Ternary Semiconductors: The Importance of the Octet Rule." *Phys. Rev. B Physical Review B*. Print.

[15] Phys Rev B 91, 205207, 2015

[16] Cho, A. Y.; Arthur, J. R.; Jr (1975). "Molecular beam epitaxy". *Prog. Solid State Chem.* 10: 157–192

[17] T. D. Brown, PhD Diss, GaTech 2003 – attributed to A. S. Brown in Encyclopedia of Advanced Materials 1990.

[18] R.E. Honig and D.A. Kramer, “Vapor Pressure Data for the Solid and Liquid Elements” RCA Review 30, 285-305 (1969).

[19] Materer, N., Rory S. Goodman, and Stephen R. Leone. "Comparison of electron cyclotron resonance and radio-frequency inductively coupled plasmas of Ar and N2: Neutral kinetic energies and source gas cracking." *Journal of applied physics* 83.4 (1998): 1917-1923.

[20] Correrra, L. *High Tc Superconductor Thin Films*. 2012. 297. Print.

[21] Rhodes, R. (1995). *The Making of the Atomic Bomb*. Simon and Schuster

[22] Nathaniel Feldberg, $ZnSnN_2$: "Growth and Characterization of an Earth Abundant Element Material with Order Dependent Properties." PhD thesis, University at Buffalo, 2015

[23] L. C. Mcintyre, Jr, M. D. Ashbaugh and J. A. Leavitt (1987). Limits on the Accuracy of Stoichiometry Determined by Rutherford Backscattering Using Computer Peak Fitting.. MRS Proceedings, 93, 401 doi:10.1557/PROC-93-401.

[24] Narang, Prineha, Shiyou Chen, Naomi C. Coronel, Sheraz Gul, Junko Yano, Lin-Wang Wang, Nathan S. Lewis, and Harry A. Atwater. "Bandgap Tunability in Zn(Sn,Ge)N 2 Semiconductor Alloys." *Adv. Mater. Advanced Materials* (2013): 1235-241. Print.